Available online at www.sciencedirect.com

ScienceDirect

Procedia CIRP 00 (2017) 000–000

www.elsevier.com/locate/procedia

The 50th CIRP Conference on Manufacturing Systems

Variation analysis of automated wing box assembly

Otto J Bakker[a,*], Atanas A Popov[a], Svetan M Ratchev[a]

[a]*Advanced Manufacturing Technology Research Group, Faculty of Engineering, University of Nottingham, University Park Campus, Nottingham, NG7 2RD, UK*

[*] Corresponding author. Tel.: +44 (0)115 74 86132; fax: +44 (0)115 95 13800. *E-mail address:* OttoJan.Bakker@Nottingham.ac.uk

Abstract

Manufacturing process variability is a major issue of concern in high value industries. Manufacturing small batches and in some cases batches of one is a very expensive process with specific requirements for manufacturing operations, tooling and fixturing and their level of automation and informatics provision. The automation targets cost reduction and a counterbalancing of the ever lower numbers of skilled shop floor workers. However, these small series typically are products that contain complex and compliant parts, and often also a high number of parts and components. The automation of this type of low-volume high-value production can be a daunting task.

Each process has its own key parameters that are required to be within a certain tolerance band in order to ensure product quality, such as e.g. the dimensions and location of assembly mating features. Dimensional quality assurance is typically done with in-process measurement, or the measurement of certain key characteristics (KCs) in the current setup, but a special setup may have to be used in a measurement-only step in the manufacturing process. Each manufacturing stage introduces errors stemming from uncertainties in the fixturing, used processes etc. These errors will propagate in downstream stages and can even worsen errors introduced in the latter stages.

The paper presents a new generic methodology for the use of stream of variation (SoV) analysis within a Smart Factory environment such as the Evolvable Assembly Systems (EAS) framework. The research is demonstrated using a simplified case study of one of EAS demonstrators for an aircraft wing box assembly. The wing box assembly and its KCs are described using formal representation. The SoV model is applied to model and simulate the assembly process. The simulation results are then analysed to predict, control and minimise the error propagation coming from uncertainties in process and equipment.

Peer-review under responsibility of the scientific committee of The 50th CIRP Conference on Manufacturing Systems.

Keywords: Variation analysis; aerospace manufacture; multistage assembly process

1. Introduction

The variability in manufacturing process outcome is a major issue of concern in the aerospace industries. Today's markets are characterized by high fluctuations in demand and a high level of customization, resulting in the manufacturing of small batches and even one offs. In addition, aerospace components are relatively large, yet have very low dimensional tolerances, making the dimension to tolerance ratio larger than most mechanical assemblies. In addition, individual parts are made as light as possible and therefore are very compliant. It requires a large number of fixtures to keep all the components and sub-assemblies in shape, until after the entire aircraft is assembled, which is remarkably stiff [1]. Something similar holds for the automotive industry, since cars are for a large degree made of sheet-metal sub-assemblies, which are also highly compliant until the entire assembly is carried out [1,2]. Apart from the production volume, aerospace assembly differs from automotive assembly in one important aspect: for a number of reasons it is considered best to have aircraft components fastened by rivets or bolts. This requires the drilling of tens or hundreds of thousands of holes. Due to lightning strike and structural requirements these holes cannot be too large, thus tightening the tolerances. This makes part-to-part assembly problematic, however the application of part-to-part assembly would introduce large cost and other technical benefits to aerospace manufacturers.

For this reason, the study of variations in aerospace manufacture and assembly has received specific attention from the research community, e.g. [3–7]. Maropoulos *et al.* [5] have developed a metrology assisted assembly method. Bakker *et al.* [6] studied the reclamation of a trailing edge hinge line key characteristic (KC) using a reconfigurable fixture and Vaughan *et al.* [7] studied the use of a variation aware algorithm for the placement of ribs in an aircraft wing-box assembly. In the automotive sector, two more formal approaches to assembly can be found, and are written up in two monographs. The first is called Stream-of-Variation (SoV) [2]. This approach concerns fixturing errors for 2D assemblies, the largest source of error in automotive industry [2]. The other approach is named state-transition models [1], and mostly studies variation in part dimensions. Applying constraint equations, Huang *et al.* [8,9] have extended SoV to 3D and also to incorporate errors coming from variation in part dimensions. Apart from a few exceptions, these methods are not widely applied to study aerospace assem-

Peer-review under responsibility of the scientific committee of The 50th CIRP Conference on Manufacturing Systems.

bly, see e.g. [10,11]. However, using more formalised forms of description and modelling of aerospace assemblies would unlock the benefits of recent advances in the application cyber-physical systems in automation. This papers seeks to formalise a state-space description for aerospace assembly, with as specific case study the structural assembly of a wing-box.

The paper is organized as follows. In the Methodology section, firstly the an assembly method and an improvement are discussed in Section 2.1. Subsequently the assembly KCs are studied in Section 2.2. The majority of the Methodology section is devoted to the establishing of the stream-of-variation model in state-space notation, this can be found in Section 2.3. Furthermore, the modelling of the shimming process that ensures that top and bottom panels are assembled according to specification is done in Section 2.4. The simulation and results are discussed in Section 3. Conclusions, observations and intended extension of the work are given in Section 4.

2. Methodology

2.1. Assembly methods

2.1.1. Assembly strategy 1

In order to establish the stream of variation model, firstly the assembly methods need to be discussed. Typically, a wing-box assembly starts with building the trailing edge (TE) sub-assembly. From there the TE spar is mounted on the TE sub-assembly. The next steps are adding the ribs and the leading edge (LE). After this, the panels at the top and bottom sides of the wing-box are mounted to the TE spar-rib-LE spar assembly. In the model analyzed in this work, the specific order can be seen in Fig. 2. N.B. this and the other assembly strategy are two possible assembly sequences, and do not necessarily form best-practice, or express the view of the authors on assembly strategies. In the figure the approximate location of the primary and secondary locating points for the assembly are drawn as the concentric circles (pin-hole) and the pin-slot respectively. In the first station the TE spar and the rib attachment angle are assembled together. The locating and measurement points for all the parts in the assembly can been seen in Fig. 1 and the numerical values for each of these points are given in Table 1. In Station 1 P_1 and P_2 are used to hold the TE spar, and P_3 and P_4 are used to rib attachment angle.

Going to Station 2, the TE spar-rib attachment angle sub-assembly is held by P_1 and P_1, as can be seen in Fig. 2 and rib is held by P_9 and P_{10}. At this station, the rib is assembled to the TE spar-rib attachment angle sub-assembly. Parallel to this the other rib attachment angle, held by P_7 and P_8 is assembled onto the LE spar held by P_5 and P_6, which are the main locating points for this sub-assembly.

At the third station, the second sub-assembly held by locating points P_5 and P_6 is mounted onto the main sub-assembly, held by P_1 and P_2.

At the fourth station, the sub-assembly is held for measurement by P_1 and P_6. For this station there is an output matrix $\mathbf{C}$. The output matrix relates the deviations of the measured points to the deviated states. Based on these measurements, shims are made and attached on the top and the bottom of the TE spar-rib-LE spar sub-assembly.

In Station 5 and 6, the top and bottom skin, respectively part

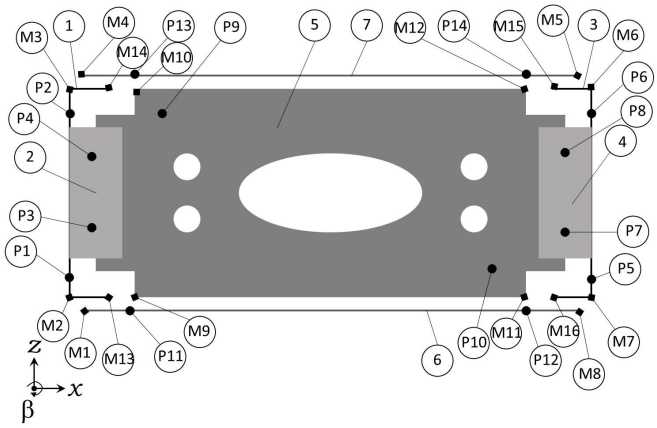

Fig. 1. Simplified cross sectional model of a wing-box assembly, N.B. stringers, clips and cut-outs in the rib to accommodate for the stringers are omitted to simplify the drawing and some of the calculations. P_i is locating point i, M_i is measurement point i. Parts are: (1) trailing edge spar, (2) rib attachment angle, (3) leading edge spar, (4) rib attachment angle (5) rib, (6) top skin (panel) 7 bottom skin (panel).

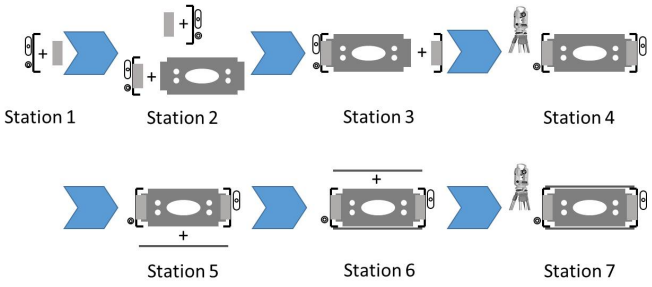

Fig. 2. Assembly sequence of the wing-box cross-section using assembly strategy 1.

6 and 7 in Fig. 1 are mounted on the TE spar-rib-LE spar sub-assembly, held by locating points P_1 and P_6 (Note that the outward normal of the bottom skin points in positive z-direction and the outward normal of the top skin points in negative z-direction in Fig. 1.)

At the 7th station, the whole wing-box assembly is held for measurement by P_1 and P_6. At this station the gaps between the panels at the top and bottom side of the wing-box is measured.

2.1.2. Assembly strategy 2

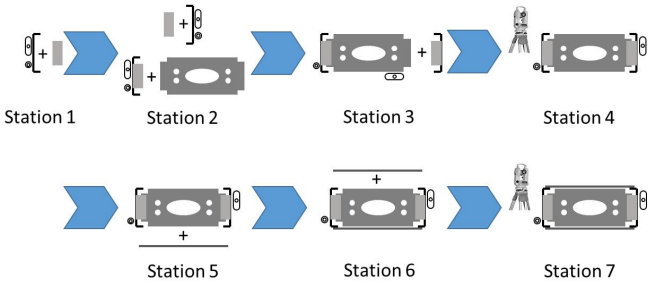

Fig. 3. Assembly sequence of the wing-box cross-section using assembly strategy 2.

As can be seen in Fig. 3, assembly strategy 2 is very similar to assembly strategy 1, with the difference that in Station 3, the secondary locating point is moved from the TE spar to the

Table 1. Nominal position of the locating and measurement points.

Point	x [mm]	z [mm]
P_1	0	32
P_2	0	137
P_3	15	57
P_4	15	112
P_5	495	32
P_6	495	137
P_7	480	57
P_8	480	112
P_9	70	137
P_{10}	425	32
P_{11}	123.75	0
P_{12}	371.75	0
P_{13}	123.75	169
P_{14}	371.75	169
M_1	1.1	0
M_2	0	2
M_3	0	167
M_4	1.1	169
M_5	493.9	169
M_6	495	167
M_7	495	2
M_8	493.9	0
M_9	40	2
M_{10}	40	167
M_{11}	455	2
M_{12}	455	167
M_{13}	30	2
M_{14}	30	167
M_{15}	465	167
M_{16}	465	2

rib, thus offering more support to what in reality is a compliant structure, and also increasing the distance between the locating points, making it more robust against geometrical errors in the fixturing points. This would be a possibility if the rib holding fixture can be retained during the assembly.

2.2. Assembly key characteristics

The key characteristics in a typical structural wing-box assembly are the gaps, flush and steps of the panels to create an aerodynamically smooth airfoil. In this work, this is analyzed by studying the variation in x-direction between the panels and the spars. In Fig. 1, it can be seen that measurement points M_1-M_8 are used for this.

Another important aspect is the application of shim (possibly in combination with fettling (a material removal process)) to make the mating features fit. In this work, only shimming is considered. Typically, engineering/stress departments allow only small shims, as large shims endanger the structural integrity of any construction.

2.3. Establishing a stream-of-variation model

For stream-of-variation models, the state-space formulation is written slightly different than usual, the left hand side of the equation contains the *current* state, and the state matrix $\mathbf{A}$ considers the state at the previous station. Ignoring the higher order terms, process disturbances and measurement noise, the state space formulation in [2, Eq. (6.39), (6.40)] is as follows:

$$\mathbf{x}_k = \mathbf{A}_{k-1}\mathbf{x}_{k-1} + \mathbf{B}_k\mathbf{u}_k \quad k = 1, 2, \ldots, N; \tag{1}$$

$$\mathbf{y}_k = \mathbf{C}_k\mathbf{x}_k \quad \{k\} \subset \{1, 2, \ldots, N\}. \tag{2}$$

Hence, matrices $\mathbf{A}$, $\mathbf{B}$ and $\mathbf{C}$ are assembled for each stage k, and furthermore, they are assembled for each part in the assembly. The state-vector $\mathbf{x}_k$ gives the translational and rotational information for stage k for each part. In the 2D example shown in Fig. 1, there are 7 parts, which each have the 2 translational (x, z) and 1 rotational (β) degree of freedom, hence there are 21 states.

2.3.1. Establishing the state matrix

State matrix $\mathbf{A}_{k-1}$, which describes the re-orientation error coming from previous stages can be defined as

$$\mathbf{A}_{k-1} = \mathbf{I} + \mathbf{H}_{k-1}$$

As mentioned before, the state matrix is square and for the 2D case and rigid parts, its rows and columns span the number of states, which is three times the number of the parts in the assembly. The intermediate combination matrix $\mathbf{H}_{k-1}$ is defined to be:

$$\mathbf{H}_{k-1} = [\ (\mathbf{H}_{1,k}\mathbf{W}_2(s,k))^T \quad (\mathbf{H}_{2,k}\mathbf{W}_2(s,k))^T \quad \ldots \quad \ldots \quad (\mathbf{H}_{n_p,k}\mathbf{W}_2(s,k))^T\ ]^T$$

for $k \geq 2$. The selecting matrix $\mathbf{W}_2(s,k)$ can be defined as:

$$\mathbf{W}_2(s,k) = \begin{bmatrix} \mathbf{W}_{1,1} & \mathbf{W}_{1,2} & \ldots & \mathbf{W}_{1,n_p} \\ \mathbf{W}_{2,1} & \mathbf{W}_{2,2} & \ldots & \mathbf{W}_{2,n_p} \end{bmatrix}_{6\times 3n_p},$$

where

$$\mathbf{W}_{j,g} = \begin{cases} \mathbf{I}_{3\times 3} & \text{if } (j,g) = (1,J) \text{ or } (2,G) \\ \mathbf{0}_{3\times 3} & \text{otherwise} \end{cases}$$

I.e. if $J = 3$, $\mathbf{W}_{1,3} = \mathbf{I}_{3\times 3}$, etc. etc. and if $G = 3$, $\mathbf{W}_{2,3} = \mathbf{I}_{3\times 3}$ etc. etc. Then on individual part level, $\mathbf{H}_{i.k}$ becomes

$$\mathbf{H}_{i,k} = [\ \mathbf{B}_2^{i,k}\mathbf{F}_1 \quad \mathbf{B}_2^{i,k}\mathbf{F}_2\ ]$$

where building block matrix $\mathbf{B}_2^{i,k}$ is:

$$\mathbf{B}_2^{\mathbf{i.k}} = \begin{cases} \mathbf{R}_1^{LS_{1,s,k},LP_{1,i,k}}\mathbf{R}_4^{k-1,k}\mathbf{W}_2(s) & \text{if } k \geq \xi_i, \\ \mathbf{0} & \text{if } k < \xi_i. \end{cases}$$

$LS_{1,s,k}$ and $LP_{1,i,k}$ are the primary locating points of the current assembly fixture and individual part respectively. Selection matrices $\mathbf{F}_1$ and $\mathbf{F}_2$ are defined to be:

$$\mathbf{F}_1 = \begin{bmatrix} 1 & 0 & 0 \\ 0 & 1 & 0 \\ 0 & 0 & 0 \\ 0 & 0 & 0 \end{bmatrix}; \qquad \mathbf{F}_2 = \begin{bmatrix} 1 & 0 & 0 \\ 0 & 1 & 0 \\ 0 & 0 & 0 \\ 0 & 0 & 0 \end{bmatrix} \mathbf{R}_1^{LP_{1,G,k},LP_{2,G,k}}$$

Where G is the index of the part where the secondary locating point of the assembly rests. The part reorientation matrix $\mathbb{R}_4^{k,k-1}$ that describes the error between the two stages is defined as:

$$\mathbf{q}_{s,k} = \mathbf{R}_4^{-k,k} \begin{bmatrix} \delta LS_{1,s,k-1}(x) \\ \delta LS_{1,s,k-1}(z) \\ \delta LS_{2,s,k-1}(x) \\ \delta LS_{2,s,k-1}(z) \end{bmatrix},$$

where

$$\mathbf{R}_k^{k-1,k} = \begin{bmatrix} -1 & 0 & 0 & 0 \\ 0 & -1 & 0 & 0 \\ \frac{-\sin\beta_{s,k}}{SD_{s,k}} & \frac{\cos\beta_{s,k}}{SD_{s,k}} & \frac{\sin\beta_{s,k}}{SD_{s,k}} & -\frac{\cos\beta_{s,k}}{SD_{s,k}} \end{bmatrix}.$$

2.3.2. Establishing the input matrix

The input matrix $\mathbf{B}$, which describes the errors introduced by the current fixtures, can be established with [2, Eq. (6.11), (6.30)]:

$$\mathbf{B}_1^{\mathbf{i,k}} = \begin{cases} \mathbf{R}_1^{LS_{1,s,k},LP_{1,i,k}} \mathbf{R}_3^{s,k} \mathbf{W}_1(s) & \text{if } k \geq \xi_i, \\ \mathbf{0}_{3\times 4n_k} & \text{if } k < \xi_i. \end{cases}$$

Here ξ_i is the index of the station where the part is introduced. The rotation matrix $\mathbf{R}_1$ get the inputs from $LS_{1,s,k}$, the primary locating point of the total assembly in stage k and $LP_{1,i,k}$ which is the primary locating point of the part under consideration. Where selection $\mathbf{W}_1(s)$ is given in [2, Eq. (6.12)]:

$$\mathbf{W}_1(s) = \begin{bmatrix} \Delta_{1s}\mathbf{I}_{4\times4} & \Delta_{2s}\mathbf{I}_{4\times4} & \dots & \Delta_{hs}\mathbf{I}_{4\times4} \end{bmatrix},$$

this matrix selects the locator pair of the part under consideration. The deviation $\mathbf{q}_{s,k}$ due to the fixturing error of the assembly fixture is related to the primary and secondary locating points as follows:

$$\mathbf{q}_{s,k} = \mathbf{R}_3^{s,k} \begin{bmatrix} \delta LS_{1,s,k}(x) \\ \delta LS_{1,s,k}(z) \\ \delta LS_{2,s,k}(x) \\ \delta LS_{2,s,k}(z) \end{bmatrix} = \mathbf{R}_3^{s,k} \cdot \mathbf{u}_{s,k}$$

Where fixturing error matrix $\mathbf{R}_3^{s,k}$ is defined as:

$$\mathbf{R}_3^{s,k} = \begin{bmatrix} 1 & 0 & 0 & 0 \\ 0 & 1 & 0 & 0 \\ \frac{\sin\beta_{s,k}}{SD_{s,k}} & -\frac{\cos\beta_{s,k}}{SD_{s,k}} & -\frac{\sin\beta_{s,k}}{SD_{s,k}} & \frac{\cos\beta_{s,k}}{SD_{s,k}} \end{bmatrix}$$

Here SD is the Euclidean distance between the two locating points, which in our case is the absolute distance calculated with Pythagoras. The total input matrix $\mathbf{B}_k$ for the current, i.e. k-th station should then be assembled for each part as follows [2, Eq. (6.30)]:

$$\mathbf{B}_k = \begin{bmatrix} (\mathbf{B}_1^{1,k})^T & (\mathbf{B}_1^{2,k})^T & \dots & (\mathbf{B}_1^{n_k,k})^T \end{bmatrix}^T$$

2.3.3. Establishing the output matrix

Define the deviations in the measured dimensions as output $\mathbf{y}_k$ at stage k as

$$\mathbf{y}_k \equiv \begin{bmatrix} \mathbf{y}_1^T & \dots & \mathbf{y}_{m_k}^T \end{bmatrix}^T = \mathbf{C}_k \mathbf{x}_k \tag{3}$$

Output matrix $\mathbf{C}_k$, which relates the measured deviations to the deviation state $\mathbf{x}_{k-1}$ has as many columns as there are states in the assembly, and two times as many rows as there are measurement points in the assembly stage. For measurement point j on part i at assembly station k holds:

$$\mathbf{y}_{i,k}^j = \mathbf{R}_0^{LP_{1,i,k},SP_{j,i}} \mathbf{x}_{i,k},$$

where the selective rotation matrix is defined as

$$\mathbf{R}_0^{LP_{1,i,k},SP_{j,i}} = \begin{bmatrix} 1 & 0 & 0 \\ 0 & 1 & 0 \end{bmatrix} \mathbf{R}_1^{LP_{1,i,k},SP_{j,i}}$$

The part level output $\mathbf{C}_{i,k}$ becomes then:

$$\mathbf{C}_{i,k} = \begin{bmatrix} \mathbf{R}_0^{LP_{1,i,k},SP_{1,i}} \\ \mathbf{R}_0^{LP_{1,i,k},SP_{2,i}} \\ \vdots \\ \mathbf{R}_0^{LP_{1,i,k},SP_{m_{i,k},i}} \end{bmatrix}$$

Which sits as block diagonal on matrix $\mathbf{C}_k$ in Eq. (3):

$$\mathbf{C}_k = \begin{bmatrix} \mathbf{C}_{1,k} & \mathbf{0} & \dots & \mathbf{0} \\ \mathbf{0} & \mathbf{C}_{2,k} & \dots & \mathbf{0} \\ \vdots & \vdots & \ddots & \vdots \\ \mathbf{0} & \mathbf{0} & \dots & \mathbf{C}_{1,k} \end{bmatrix}$$

2.4. Shimming after measurement station 4

In order to ensure the top and bottom panel are actually mounted on a flat surface, the maximum positive deviation in z-direction at measurement points $\{M_3, M_{14}, M_{10}, M_{12}, M_{15}, M_6\}$ and the maximum negative deviation at measurement points $\{M_2, M_{13}, M_9, M_{11}, M_{16}, M_7\}$ (see Fig 1) are found the with respectively the `max` and `min` commands in MATLAB. For the simulation in Section 3, these maximum values are recorded in Tables 2 and 3. If we assume that these measurement points are all placed on the outer edges of the spar flanges and rib brackets, the amount of applied shim between measurement points l and m can calculated as follows:

$$\frac{1}{2}(\|\delta z_{\max} - \delta z_l\| + \|\delta z_{\max} - \delta z_m\|)MD. \tag{4}$$

This is another way to look at the shimming process [12]. Where $\delta z_{\max}$ is the maximum found deviation and MD is the Euclidean distance between the measurement points l and m.

When the variation in the assembly is calculated, the fixtures that hold the panels (parts 6 and 7 in Fig. 1) are in Station 5 and 6 are given an offset in z-direction with the magnitude of found maximum deviation. This ensures that the panels are mounted on top of the shim and horizontally, without introducing extra constraint equations in the form of wrench matrices [8,9].

3. Results and discussion

3.1. Simulation

The steps for the simulation are the following: (1) Establish $\mathbf{A}_{k-1}$, $\mathbf{B}_k$ for stations 1-7; $\mathbf{C}_k$ for measurement stations 4 and 7. (2) $\mathbf{x}_0 = \mathbf{0}$; $\mathbf{u}_1$, $\mathbf{u}_2$, $\mathbf{u}_3$ and $\mathbf{u}_4$ are 28 by 1 vectors that are random for a normal distribution of values between 0 and 0.1. Apart from the x-values for P_1 to P_8 in Fig. 1. (3) The measured deviation $\mathbf{y}_4$ for M_2, M_3, M_6, M_7, $M_9 - M_{16}$ in Fig 1, is calculated for station 4. (4) The difference between the largest and smallest values in z-directions on top and bottom sides of the spar is calculated to establish the required shim thickness. (5) The fixturing points for the top and bottom cover, see Fig. 1, in z-direction are corrected with the found minimum and maximum values (to avoid interference with the shims and the parts) in $\mathbf{u}_1$-$\mathbf{u}_7$. (6) The measured deviations $M_1 - M_8$ at station 7 can be calculated. (7) The applied shim is the distance between two points, e.g. M_{10} and M_{12} for the bottom side of the rib multiplied by the average of the shim thickness at these both points.

Table 2. statistical summary of strategy 1.

σ maximum deviation – top	0.7970 mm
σ maximum deviation – bottom	0.8305 mm
σ applied shim – top	304.2560 mm^3/mm
σ applied shim – bottom	320.2311 mm^3/mm
2-norm maximum shim – top	11.2059 mm^2
2-norm maximum shim – bottom	11.9079 mm^2
2-norm applied shim – top	4774.4 mm^6/mm^2
2-norm applied shim – bottom	5225.5 mm^6/mm^2
σ gap top panel trailing edge side	0.2752 mm
σ gap bottom panel trailing edge side	0.4414 mm
σ gap top panel leading edge side	0.3230 mm
σ gap bottom panel leading edge side	0.3171 mm
2-norm gap top panel trailing edge side	2.7417 mm^2
2-norm gap bottom panel trailing edge side	4.4383 mm^2
2-norm gap top panel leading edge side	3.2286 mm^2
2-norm gap bottom panel leading edge side	3.1595 mm^2

Table 3. statistical summary of strategy 2.

σ maximum deviation – top	0.6894 mm
σ maximum deviation – bottom	0.7605 mm
σ applied shim – top	310.8978 mm^3/mm
σ applied shim – bottom	342.4093 mm^3/mm
norm maximum shim – top	8.6585 mm^2
norm maximum shim – bottom	10.3851 mm^2
norm applied shim – top	4009.3 mm^6/mm^2
norm applied shim – bottom	4769.3 mm^6/mm^2
σ gap top panel trailing edge side	0.2492 mm
σ gap bottom panel trailing edge side	0.2305 mm
σ gap top panel leading edge side	0.3834 mm
σ gap bottom panel leading edge side	0.3628 mm
norm gap top panel trailing edge side	2.4858 mm^2
norm gap bottom panel trailing edge side	2.3308 mm^2
norm gap top panel leading edge side	3.8153 mm^2
norm gap bottom panel leading edge side	3.6105 mm^2

It is assumed that because we are working with robotic assembly, there is a variation of the locating points with a Gaussian distribution and a maximum of 0.1 mm in both directions, as robots in our laboratory when assisted by metrology can achieve an accuracy of 0.1 mm. 100 simulations of each strategy where made.

3.2. Results for simulation strategy 1

In Table 2 the summary of the statistics from the analysis of assembly strategy 1 can be found. In the first section one can find the standard deviation of the maximum deviation at the top and bottom of the assembly. See Section 2.4 for the measurement points.

In the second section of Table 2 the 2-norm, which is the sum of the squared elements of the vector containing the hundred values of each of these parameters is given. In the third and fourth sections of the table, the deviation and the 2-norm of the gap, i.e. the distances in x-direction between M_1 and M_2, M_3 and M_4, M_5 and M_6, and M_7 and M_8 are given.

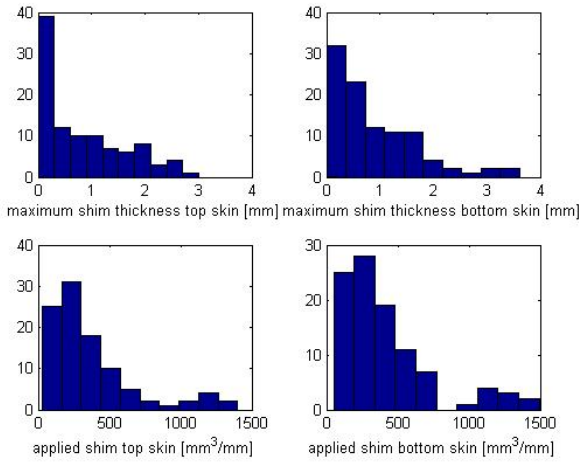

Fig. 4. Maximum deviation at top and bottom of spars and rib and applied shim histograms for assembly strategy 1.

In Fig. 4 the histograms for the 100 simulations for the the maximum deviation at the top and bottom skin are given, as well as the histograms for the applied shim. Similar to the results in [12], it can be seen that the shim in the second bracket uses up more material, despite it occurs less frequent: the increase in thickness is larger than the lower number of applied shims in that thickness bracket.

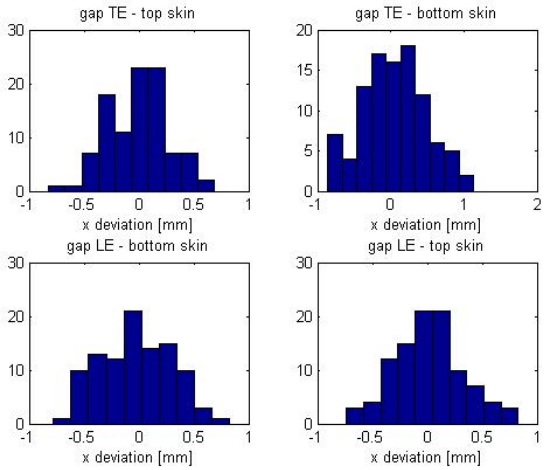

Fig. 5. Histograms of the horizontal 'gap' between panels and spar for assembly strategy 2.

In Fig. 5 the histograms for the gaps, i.e. the distances in x-direction between M_1 and M_2, M_3 and M_4, M_5 and M_6, and M_7 and M_8 can be found.

3.3. Results for simulation strategy 2

The summary of the statistics from the analysis of assembly strategy 2 is given in Table 3. In the first section the standard deviation of the maximum deviation at the top and bottom of the assembly can be found.

The 2-norm, which is the sum of the squared elements of the vector containing the hundred values of each of these variables is given can be found in the second section of Table 3. In this table, in the third and fourth sections, the deviation and the 2-norm of the gap, i.e. the distances in x-direction between M_1 and M_2, M_3 and M_4, M_5 and M_6, and M_7 and M_8 are shown.

The histograms for the 100 simulations for the the maximum deviation at the top and bottom skin, as well as the histograms for the applied shim can be found in Fig. 6

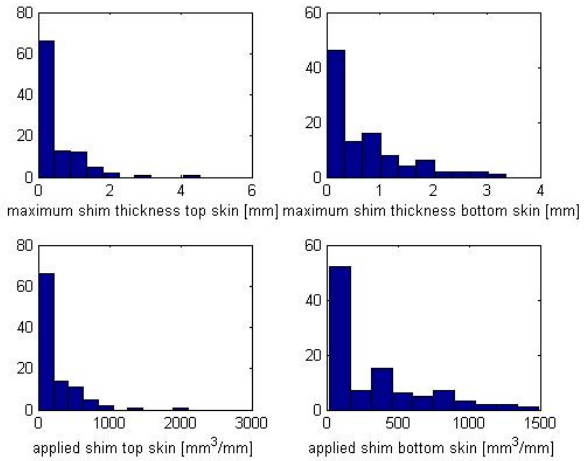

Fig. 6. Maximum deviation at top and bottom of spars and rib and applied shim histograms for assembly strategy 2.

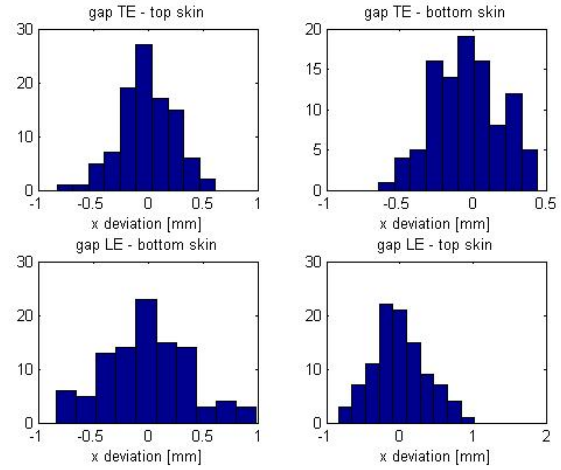

Fig. 7. Histograms of the horizontal 'gap' between panels and spar for assembly strategy 2.

The histograms for the gaps, i.e. the distances in x-direction between M_1 and M_2, M_3 and M_4, M_5 and M_6, and M_7 and M_8 can be seen in Fig. 7.

3.4. Comparison of strategy 1 and 2

Firstly, it should be mentioned that the histograms, shown in Figs 4, 4, 6 and 7 are not very smooth. This is because the 100 simulations are relatively few in number, but it gives a more realistic approach to simulations, since aerospace assembly is characterized by relatively low numbers when compared to automotive or consumer electronics industry.

As mentioned, the locating points for the assembly fixture are further apart, thus making the assembly fixture more robust. And it can be seen that, as expected, assembly strategy 2 performs better than strategy 1: the standard deviation for the vertical variation, when comparing the strategies, given in the first sections of Table 2 and 3 is smaller for strategy 2. Similar for the 2-norm for the shimming criteria and the gaps. The same can be observed visually when looking at the histograms in Figs 4, 4, 6 and 7.

4. Conclusions and future work

A stream of variation (SoV) modelling framework has been established to model the structural assembly of a wing-box. Using some assumptions and simplifications the model can be used to predict the key characteristics: amount of shim required and the gap between the panels in the wing-box assembly. Additionally, the model can used to study changes in the assembly strategy: it quantified that placing a locator to a more robust, actually led to a better assembly fixture layout.

The SoV model can be extended for use in sensitivity studies and variation source diagnosis [2].

The intention of the authors is to extend the model along the lines of Refs [1,8,9] to a model that can capture: 3D parts, part elastic compliance, part dimensional variation, and feed-forward control to reduce the variation in the wing-box assembly. Parallel to that the model will be evaluated in the new future automated robotic aerospace assembly cell at The University of Nottingham manufacturing labs.

Acknowledgements

The reported research is part of the Evolvable Assembly Systems programme, funded by the UK Engineering and Physical Science Research Council, the support of which is greatly appreciated.

References

[1] Whitney D. Mechanical Assemblies: Their Design, Manufacture, and Role in Product Development, New York / Oxford: Oxford University Press; 2004.
[2] Shi J., Stream of Variation Modeling and Analysis for Multistage Manufacturing Processes, Boca Raton, Fl: CRC / Taylor & Francis; 2007.
[3] Saadat M and Cretin C. Dimensional variations during Airbus wing assembly, Assem Autom, 2002. 22 (3): 270-276.
[4] Saadat M, Sim R and Najafi F. Prediction of geometrical variations in Airbus wingbox assembly, Assem. Autom, 2007, 27 (4): 324-332.
[5] Maropoulos PG, Muelaner JE, Summers MD, and Martin OC. A new paradigm in large-scale assembly - research priorities in measurement assisted assembly, Int J Adv Manuf Technol, 2013, 70 (1-4): 621-633.
[6] Bakker, O, Jayaweera, N, Martin, O, Turnock, A et al., Fixturing and Tooling for Wing Assembly with Reconfigurable Datum System Pickup, SAE Technical Paper 2011-01-2556, 2011, doi:10.4271/2011-01-2556.
[7] Vaughan, D, Bakker, O, Branson, D, and Ratchev, S. Variation Aware Assembly Systems for Aircraft Wings, SAE Technical Paper 2016-01-2106, 2016, doi:10.4271/2016-01-2106.
[8] Huang W, Lin J, Bezdecny M, Kong Z, Ceglarek D. Stream-of-Variation Modeling – Part I: A Generic Three-Dimensional Variation Model for Rigid-Body Assembly in Single Station Assembly Processes. ASME. J. Manuf. Sci. Eng. 2007;129(4):821-831. doi:10.1115/1.2738117.
[9] Huang W, Lin J, Kong Z, Ceglarek D. Stream-of-Variation (SOVA) Modeling – Part II: A Generic 3D Variation Model for Rigid Body Assembly in Multistation Assembly Processes. ASME J Manuf Sci Eng, 2007;129(4):832-842. doi:10.1115/1.2738953.
[10] Zhang T and Shi J. Stream of Variation Modeling and Analysis for Compliant Composite Part Assembly – Part I: Single-Station Processes, ASME J Manuf Sci Eng, 2016, 138: 121003-1–121003-15
[11] Zhang T and Shi J. Stream of Variation Modeling and Analysis for Compliant Composite Part Assembly – Part II: Multistation Processes, ASME J Manuf Sci Eng, 2016, 138: 121004-1–121004-15
[12] Lee R. Evaluation of Shimming Options with Applications to JSF, Technical Report (preliminary), Advanced Affordability Initiative; 1999.